DOI: 10.1002/ejic.201000517

Synthesis and Photophysical Properties of Ln^{III}–DOTA–Bipy Complexes and Ln^{III}–DOTA–Bipy–Ru^{II} Coordination Conjugates

Miguel Vázquez López,*[a] Svetlana V. Eliseeva,[b] José M. Blanco,[a] Gustavo Rama,[a] Manuel R. Bermejo,[a] M. Eugenio Vázquez,[c] and Jean-Claude G. Bünzli*[b,d]

Keywords: Lanthanides / Ruthenium / Luminiscence / Energy transfer / Supramolecular chemistry

The synthesis and the systematic and comparative photophysical study of a series of visible (Eu^{III}, Tb^{III}) and NIR-emitting (Nd^{III}, Yb^{III}) lanthanide complexes (Ln_2L) and ruthenium–lanthanide coordination conjugates (Ln_2LRu) are reported. The Gd^{III} complex, the Gd^{III}–Ru^{II} coordination conjugate, as well as the Ru^{II} complex of the ligand H_6L have also been synthesized and photophysically studied as control systems. The ligand H_6L, composed of a central bipyridine binding unit and functionalized on each 5′-position with a DOTA macrocycle, has been successfully synthesized from cyclen, 5,5′-dimethyl-2,2′-bipyridine and 1,2-ethylendiamine in a nine-step process. Detailed luminescence studies of all complexes, including the determination of the quantum yield and lifetime, were carried out on finely powdered microcrystalline samples as well as in water, deuterated water and [D_6]DMSO at ambient (295 K) and low temperature (77 K). The photophysical data corroborate the existence of energy transfer in the Ln_2L complexes and in the Nd_2LRu coordination conjugate. However, no (or at most, very little) energy transfer is takes place from the $Ru(bipy)_3$ chromophore to the Ln^{III} ion in the other Ln_2LRu heteropolymetallic complexes. Moreover, the photophysical studies reveal that all the complexes and coordination conjugates adopt different conformations and hydration states in solution and in the solid state, which influences the efficiency of the energy transfer between the bipy and/or $Ru(bipy)_3$ antennae and the Ln^{III} ions.

Introduction

The development of luminescent trivalent lanthanide complexes is an active research field[1] with important applications in laser systems,[2] in optical amplification[3] and in biological imaging and sensing.[4] The advantages of these complexes lie in their long-lived excited states (μs to ms) and long emission wavelengths (500–1550 nm) with line-like emission bands that allow unique applications.[5] However, lanthanide ions suffer from Laporte-forbidden f–f transitions, which makes direct excitation impractical unless powerful lasers are used. To overcome this problem, Ln^{III} excited states are populated through energy transfer from nearby sensitizing fluorophores that absorb at shorter wavelengths.[1] For lanthanide ions such as Tb^{III} or Eu^{III}, this requires excitation at wavelengths shorter than ≈400 nm. Since biological samples absorb heavily at the UV and visible wavelengths, the practical spectroscopic range is restricted to the red end of the visible spectrum and to the near-infrared (NIR) region; at these wavelengths the light penetrates tissues more effectively and it can therefore reach a luminescent marker inside a tissue sample. This difficulty can be circumvented by using other luminescent rare-earth cations, such as Nd^{III} or Yb^{III}, which emit in the NIR region (800–1300 nm) and which can be sensitized by using d-block transition-metal complexes, usually containing Ru^{II} or Os^{II}.[6–10] Such complexes are strong-absorbing chromophores in the visible region and possess relatively long-lived metal-to-ligand charge-transfer (MLCT) excited states, which enhance the efficiency of the sensitization process.[6,7] In this context, the extensively studied Ru^{II} complex [$Ru(bipy)_3$]$^{2+}$ is known for its outstanding chemical stability, for showing an intersystem-crossing quantum yield near unity and for its effective excitation of Nd^{III} and Yb^{III} after irradiation with visible light of up to 500 nm.[8,9]

In this paper, we report the synthesis of the bipyridine-based ligand H_6L (Scheme 1) and the systematic study of the photophysical properties in solution and in the solid state at different temperatures of the corresponding visible-light-emitting Eu^{III} and Tb^{III} and near-IR-light-emitting Nd^{III} and Yb^{III} complexes and their Ru^{II}–Ln^{III} coordina-

[a] Department of Inorganic Chemistry and Center for Research in Biological Chemistry and Molecular Materials, University of Santiago de Compostela
15782 Santiago de Compostela, Spain
E-mail: miguel.vazquez.lopez@usc.es
[b] Laboratory of Lanthanide Supramolecular Chemistry, École Polytechnique Fédérale de Lausanne, EPFL BCH
1015 Lausanne, Switzerland
[c] Department of Organic Chemistry and Center for Research in Biological Chemistry and Molecular Materials, University of Santiago de Compostela
15782 Santiago de Compostela, Spain
[d] WCU Center for Next Generation Photovoltaic Systems, Korea University
Sejong Campus, ChungNam 339-700, South Korea
Supporting information for this article is available on the WWW under http://dx.doi.org/10.1002/ejic.201000517.

tion conjugates. The Gd^{III} complex, the Ru^{II}–Gd^{III} coordination conjugate of H_6L and the Ru^{II}–H_6L complex have also been studied as control systems. The H_6L ligand is composed of a central bipyridine binding moiety functionalized on each 5′-position with a DOTA macrocycle for strong complexation of the lanthanide ions. The resulting Ln^{III} complexes are neutral, but the Ru^{II}–Ln^{III} coordination conjugates are cationic, bearing a +2 charge.

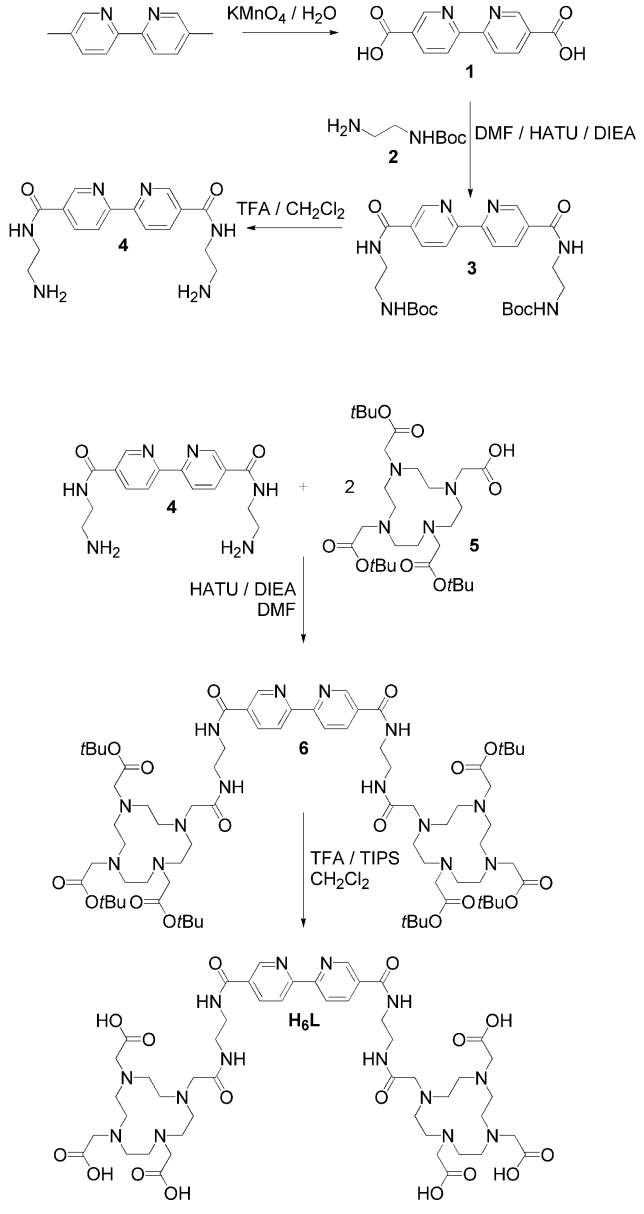

Scheme 1. Synthesis of ligand H_6L. HATU: *O*-(7-azabenzotriazol-1-yl)-*N*,*N*,*N*′,*N*′-tetramethyluronium hexafluorophosphate; DIEA: diisopropylethylamine; TIPS: triisopropylsilane; TFA: trifluoroacetic acid.

Results and Discussion

Synthetic Aspects

Ligand H_6L was prepared from the commercial reagents 1,2-ethylenediamine, 5,5′-dimethyl-2,2′-bipyridine and cyclen (Scheme 1). The first step involves the synthesis of the tri-protected DOTA derivative **5** [1,4,7-tris(*tert*-butoxycarbonylmethyl)-1,4,7,10-tetraazacyclododecane-10-acetic acid][4c] and of the monoprotected diamine **2** (*N*-*tert*-butoxycarbonyl-1,2-ethanediamine).[11] Bipyridine **3** was prepared by oxidizing 5,5′-dimethyl-2,2′-bipyridine with potassium permanganate in water, followed by condensation with monoprotected diamine **2**. Subsequent deprotection of **3** with TFA in dichloromethane followed by condensation with macrocycle **5** resulted in the protected ligand **6**. The last step involves deprotection of the *tert*-butyl groups in **6** with TFA/TIPS in dichloromethane to give H_6L. The free ligand was characterized by a variety of techniques, including ESI mass spectrometry, UV/Vis, IR , ^{1}H and ^{13}C NMR spectroscopy and elemental analysis.

A series of neutral dinuclear lanthanide complexes was obtained by reaction of the corresponding Ln^{III} triflate (Ln = Nd, Eu, Gd, Tb or Yb) with H_6L in water (Scheme 2). Purification of the corresponding lanthanide complexes was performed by semi-preparative reverse-phase HPLC. The analytical data of the obtained solids suggest that the lanthanide ions react with the ligand in a 2:1 molar ratio. The infrared spectra of the Ln_2L complexes are similar and display typical bands for the ν(C–C) and ν(C=O) vibrations at 1500–1700 cm^{-1} and for ν(N–H) and ν(C–H) in the range 2700–3600 cm^{-1} (Figure S1, Supporting Information). By comparing the IR spectra of the Ln^{III}-containing complexes with that of the free ligand H_6L, we observe that the ν(C=O) vibrational band for the COOH groups at 1725 cm^{-1} is shifted by ca. 100 cm^{-1} to 1620–1630 cm^{-1}, which is consistent with the deprotonation of the ligand. The presence of a broad band at 3000–3600 cm^{-1} confirms that all complexes contain water molecules. The ESI mass spectra of the Ln_2L complexes show peaks corresponding

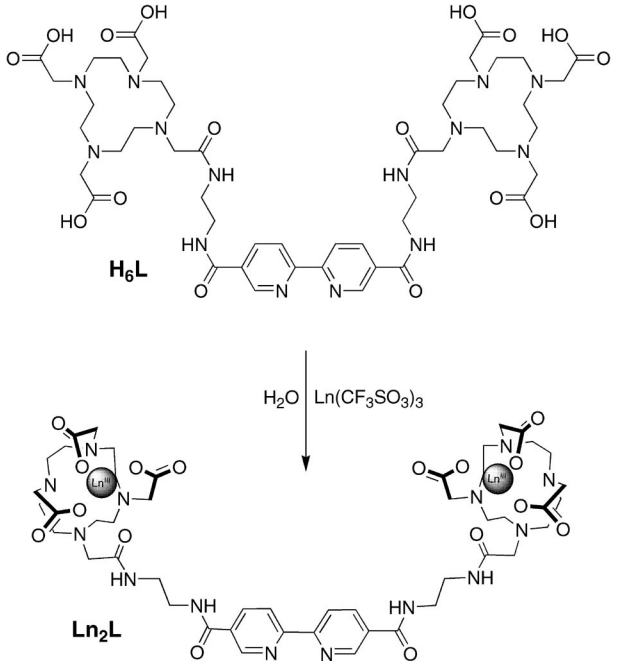

Scheme 2. Synthesis of the lanthanide complexes.

to the $[Ln_2L + H]^+$ and $[Ln_2L + 2H]^{2+}$ species. Their UV/Vis spectra in water are very similar to that of the free ligand, with two bands centred at 249 and 298 nm. Taken together, these data suggest the successful coordination of the lanthanide ions into both macrocycles of H_6L and that the Ln_2L complexes are the main species in solution.

The ruthenium(II) derivatives of Ln_2L were obtained by reacting *cis*-bis(2,2′-bipyridine)dichlororuthenium(II) dihydrate with the corresponding Ln_2L complex in refluxing water (Scheme 3). All the ruthenium–lanthanide coordination conjugates were purified by semi-preparative reverse-phase HPLC. The analytical data of the orange solids obtained suggest that the ruthenium(II) ions react with the Ln_2L complexes in a 1:1 molar ratio. The infrared spectra of $[Ru(bipy)_2(Ln_2L)]^{2+}$ (Ln_2LRu) are very similar to those of Ln_2L, and the presence of a broad band at 3000–3600 cm^{-1} of weak intensity (Figure S2, Supporting Information) confirms that all the conjugates are hydrated. The ESI mass spectra show peaks with a correct isotopic distribution for the $[Ru(bipy)_2(Ln_2L)]^{2+}$ species. The absorption spectra of the Ln_2LRu conjugates are similar and display ligand-centred and metal-to-ligand charge-transfer bands ^{1}MLCT (see details below). These data suggest the successful coordination of the $[Ru(bipy)_2]^{2+}$ moiety to the bipyridine binding group of Ln_2L and that the $[Ru(bipy)_2(Ln_2L)]^{2+}$ cations are the major species in solution.

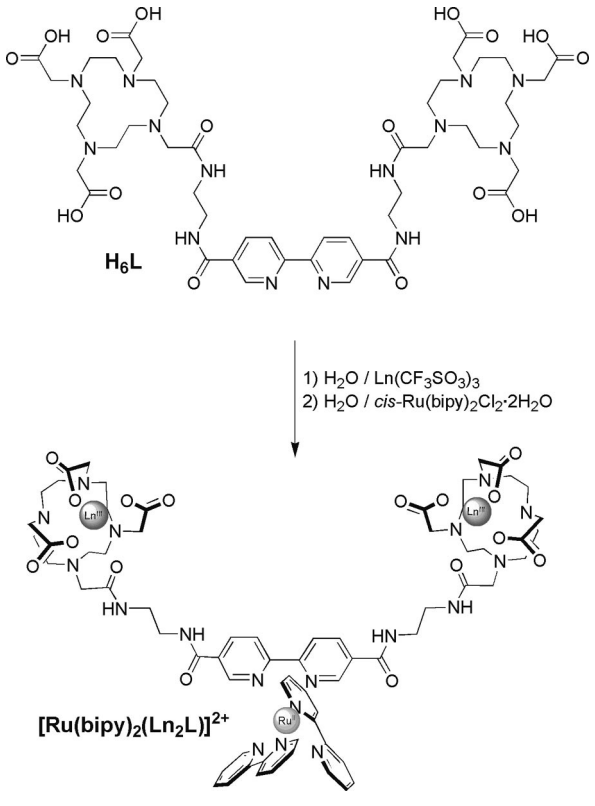

Scheme 3. Synthesis of the lanthanide–ruthenium Ln_2LRu coordination conjugates.

The ruthenium(II) derivative of H_6L was synthesized by reaction of *cis*-bis(2,2′-bipyridine)dichlororuthenium(II) dihydrate with ligand H_6L in refluxing methanol. It was purified by semi-preparative reverse-phase HPLC. The IR spectrum of $[Ru(bipy)_2(H_6L)]^{2+}$ (H_6LRu) is very similar to that of free ligand H_6L, which indicates that the two macrocycles remain protonated after complexation. The absence of a broad band at 3000–3600 cm^{-1} confirms that the complex does not contain water molecules. The ESI mass spectrum reveals a molecular ion peak with a mass and an isotopic distribution consistent with the $[Ru(bipy)_2(H_6L)]^{2+}$ species. The UV/Vis spectrum of this complex in water is very similar to those of the Ln_2LRu coordination conjugates. These data suggest the successful coordination of the $[Ru(bipy)_2]^{2+}$ moiety to the bipyridine binding group of ligand H_6L and that the $[Ru(bipy)_2(H_6L)]^{2+}$cation is the unique species in solution.

Photophysical Properties

Luminescence properties of all complexes were measured on finely powdered microcrystalline samples, as well as in water, deuterated water and [D$_6$]DMSO. In the course of the measurements, it became evident that the samples were sensitive to UV-light irradiation to an extent that depends on their composition and nature. The ligand itself is only weakly luminescent in all media and is subject to photobleaching, as evidenced by the change in colour from pale violet to brown upon irradiation of the solid-state sample at 300 nm for 30–50 min. This change is irreversible and also occurs in solution. Similar UV illumination of Ln_2L and Ln_2LRu solid state samples has no effect on the Ru^{II} emission and a very small effect (at most a 10% decrease) on the Ln^{III} emission; if photobleaching does occur, the process is reversible. In D_2O solution, the situation is different for the Ln_2L complexes: the Eu^{III}, Tb^{III} and Yb^{III} luminescence decreases by factors of ≈3.5, ≈2 and ≈1.4, respectively, while the Nd^{III} luminescence is not affected. The effect is, however, reversible (Figures S3, S4, Supporting Information) and no colour changes were observed. In view of this fact, the photophysical data reported below have been determined on freshly prepared solutions subjected to minimum irradiation by the excitation light.

Ligand-Centred Luminescence

The energy of the triplet state, $E_{T(0-0)}$, of the deprotonated ligand was determined for the reference complex Gd_2L by measuring its phosphorescence spectrum at 77 K (Figure 1). This state usually plays a crucial role in the sensitization of Ln^{III} luminescence. A higher-energy value for $E_{T(0-0)}$ relative to that of the emitting level of Ln^{III} results in an inefficient transfer, whereas when the levels are energetically too close, back energy transfer operates.[1g] At 77 K and under time-resolved detection, a weak, structured and broad emission band is detected in all media between 430 and 700 nm. The mean vibrational spacing is around 1450 cm^{-1} (Table S1 in the Supporting Information), which corresponds to C–N, C–C as well as ring breathing vibrational modes. The 0-phonon energy is redshifted from

21420 cm^{-1} in the solid state to 21740 and 21 840 cm^{-1} in [D_6]DMSO and D_2O, respectively. Therefore, the energy difference [$E_{T(0-0)}$–$E(^5D_0)$] of 4000–4400 cm^{-1} is expected to generate a moderately efficient energy transfer, while the energy level of the triplet state of the deprotonated ligand is close to the Tb($^5D_4$) level located at 20 500 cm^{-1}, so that energy back transfer is anticipated.

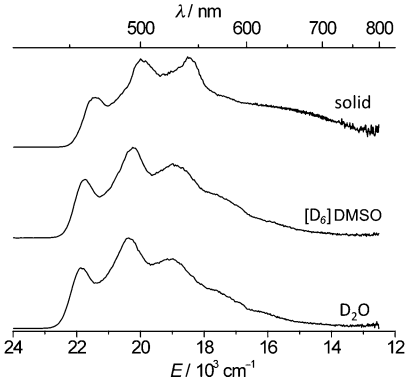

Figure 1. Corrected and normalized phosphorescence spectra of the ligand in the Gd_2L complex in different media at 77 K (λ_{ex} = 330 nm, delay time 50 μs).

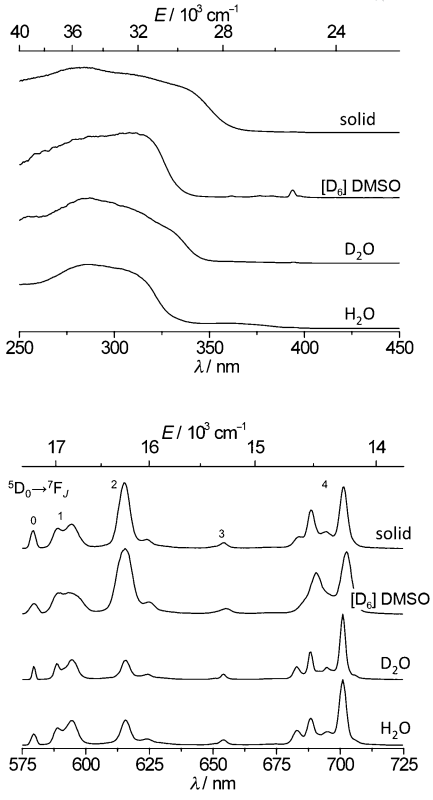

Figure 2. Corrected and normalized excitation (top) and luminescence (bottom) spectra of Eu_2L in different media at room temperature (λ_{ex} = 300 nm).

Visible-Emitting Ln_2L Complexes

Excitation spectra of Ln_2L (Ln = Eu, Tb) complexes in water, DMSO or in the solid state are quite similar and present intense broad bands in the range 250–370 nm, which correspond to the ligand electronic transitions. In addition, weak and sharp features are seen, which can be assigned to f–f transitions at ≈390 nm ($^5L_6$←$^7F_{0,1}$) for Eu_2L or in the range 350–380 nm ($^5D_3$, $^5G_6$, $^5L_{10}$, $^5G_5$, $^5D_2$, $^5G_4$, $^5L_9$←$^7F_6$) for Tb_2L. Upon excitation into the ligand levels in the range 300–330 nm, Eu_2L and Tb_2L exhibit, in all media, only characteristic narrow red or green emission assigned to $^5D_0$→^7F_J (J = 0–4) or $^5D_4$→^7F_J (J = 6–0) transitions, respectively (Figure 2 and Figures S5, S6 in the Supporting Information). The ligand-field splitting pattern shows only a small variation from one medium to the other, but significant changes in emission probabilities for different J sublevels (Tables S2 and S3, Supporting Information), in luminescent lifetimes and in quantum yields (Table 1 and Table 2) are observed. These variations can be explained by different solvation and by the flexibility of the ligand. Indeed, cyclen-based derivatives are known to form lanthanide complexes with a variety of conformational and

Table 2. Photophysical data for Tb_2L (2σ in parentheses). Excitation wavelength: 330 nm.[a]

Solvent	τ_{obs} [ms][b] 77 K	295 K	Q^L_{Tb} [%][c]
H_2O	2.47(1)	0.97(2)	1.0(1)
D_2O	3.36(3)	1.46(2)	2.3(4)
[D_6]DMSO	2.57(3)	1.88(2)	1.1(1)
Solid	0.60(3), 31(5) 1.37(2), 69(5)	0.22(1), 29(3) 0.81(2), 71 (3)	1.8(1)

[a] Data at 295 K unless otherwise stated. [b] Biexponential decays: population B_i given in %, see Experimental Section for discussion. [c] Photobleaching was observed for solutions, see text.

Table 1. Photophysical data for Eu_2L (2σ in parentheses). Excitation wavelength: 300–330 nm.[a]

Solvent	τ_{obs} [ms][b] 77 K	295 K	τ_{rad} [ms][c]	Q^{Eu}_{Eu} [%]	Q^L_{Eu} [%][d]	η_{sens} [%]
H_2O	1.62(2)	0.62(1)	6.02	10	≈0.4	3.9(6)
D_2O	3.50(5)	2.04(1)	6.14	33	1.1(2)	3.3(5)
[D_6]DMSO	3.45(5)	1.80(1)	3.21	56	1.8(3)	3.3(5)
Solid	0.79(8), 58(9)[e] 1.5(2), 42(9)[e]	0.63(2), 44(4) 1.07(1), 56(4)	3.49	27[f]	11.7(3)	43(6)

[a] Data at 295 K unless otherwise stated. [b] Biexponential decays: λ_{ex} = 355 nm, population B_i given in %, see Experimental Section for discussion. [c] Refractive index taken as equal to 1.5 for solid samples, 1.34, 1.328 and 1.476 for solutions in H_2O, D_2O and [D_6]-DMSO, respectively. [d] Photobleaching was observed for solutions, see text. [e] At 10 K. [f] Calculated using the mean lifetime: $<\tau>$ = 0.93 ms.

coordination geometries (CN = 8, 9), which depend on the experimental conditions and on the nature of the solvent and of the central ion.[12] It is also well documented that lanthanide luminescence is very sensitive to the nature of the coordination environment and its symmetry.[13] This effect is most sizeable and easy to detect for Eu^{III}. For instance, the integral intensity of the hypersensitive $^5D_0 \rightarrow {}^7F_2$ transition increases 2.8- and 2.3-fold in going from water to DMSO solutions and to the solid state, respectively.

The highly forbidden Eu($^5D_0 \rightarrow {}^7F_0$) transition gives additional clues on the metal-ion environment. Firstly, its relatively large intensity (13–19% of the magnetic dipole transition $^5D_0 \rightarrow {}^7F_1$) is typical of a coordination geometry with pseudo C_4 symmetry, an observation consistent with the ligand-field splitting pattern of the spectra. Secondly, high-resolution laser-excited excitation spectra of this transition reveal a single component for the solution samples and two for the solid-state sample (Figure 3). The corresponding parameters are listed in Table S4 (Supporting Information). These data support the existence of one species in solution, although the broadening of the transition, particularly in [D_6]DMSO, may point to an equilibrium between different conformations[12] and/or differently solvated species. For the solid-state sample, two different coordination environments are revealed, in line with elemental analysis, which points to the presence of a single water molecule in the complex. Therefore, the two coordination sites could correspond to a nine-coordinate monohydrated Eu^{III} ion and to a non-hydrated eight-coordinate metal ion. This assumption is substantiated by the energy of the two components. Indeed, this energy is correlated with the nephelauxetic effect δ_i generated by each group coordinated to the Eu^{III} ion[14] [Equation (1)].

$$\tilde{\nu}_{calc} = 17\,374 + C_{CN} \sum_{i=1}^{CN} n_i \delta_i \quad (1)$$

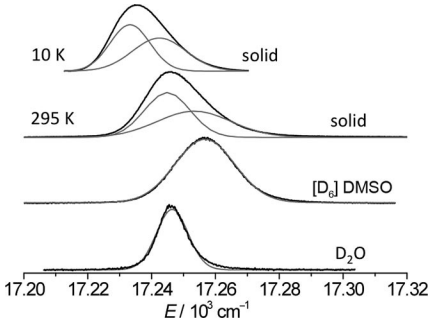

Figure 3. High-resolution scan of the $^5D_0 \leftarrow {}^7F_0$ transition upon monitoring the $^5D_0 \rightarrow {}^7F_2$ transition (610–620 nm) and Gaussian decomposition of the spectra.

where C_{CN} is a constant that depends on the coordination number and n_i the number of bound groups. By using Equation (1) with $C_9 = 1$, $\delta_{COO^-} = -17.2\ cm^{-1}$, $\delta_N = -12.1\ cm^{-1}$, and $\delta_{H2O} = -10.4\ cm^{-1}$, a value of 17246 cm^{-1} is obtained, which is in very good agreement with the experimental value of 17245 cm^{-1} (17246 cm^{-1} in D_2O). An energy of 17250 cm^{-1} is calculated for the non-hydrated eight-coordinate site ($C_8 = 1.06$, same δ_i as above), consistent with the experimental value of 17253 cm^{-1}. In highly-coordinating [D_6]DMSO solvent, the nephelauxetic effect is somewhat reduced, which leads to a 0–0 transition energy of 17257 cm^{-1}, possibly because of expansion of the coordination sphere in this solvent.[15]

Lifetime data for the $^5D_0$ level (Table 1) are compatible with the above discussion. In water, the lifetime of 0.62 ms is typical of the coordination of one water molecule: a hydration number $q = 0.96$ is indeed obtained for Eu_2L from Beeby's equation [Equation (2)].[16]

$$q(\mathrm{Eu}) = 1.2\ (\Delta k_{obs} - 0.25\text{–}0.075 q^N) \quad (2)$$

$$\Delta k_{obs} = 1/\tau_{H2O} - 1/\tau_{D2O}$$

where q^N is the number of coordinated amide groups. That is, in aqueous solution, both europium ions are hydrated and therefore nine-coordinate. When the water molecule is replaced by [D_6]DMSO, the lifetime increases to 1.80 ms. For the solid-state sample, two lifetimes are found, a short one matching the aqueous solution value, and a longer one (1.07 ms) pointing to Eu^{III} devoid of coordinated water molecules. Interestingly, the site population calculated from the luminescence decays (Table 1) is in good agreement with the predicted 1:1 ratio on the basis of elemental analysis ($\times 1H_2O$). The above model used for interpreting the $^5D_0 \leftarrow {}^7F_0$ spectra is consequently fully validated. All lifetimes are strongly temperature dependent as a consequence of vibrational deactivation processes.

Absolute luminescence quantum yields Q^L_{Eu} for Eu_2L, determined upon ligand excitation, lie in the range 0.4–1.8% for the solution samples, while they increase to up to 11.7% for the solid-state sample (Table 1). Intrinsic quantum yields are not directly measurable because of the very small molar absorption coefficients of the $^5D_J \leftarrow {}^7F_{0,1}$ transitions, but they can be estimated for the Eu^{III}-containing compounds by using the following [Equation (3)].[12]

$$Q^{Ln}_{Ln} = \frac{\tau_{obs}}{\tau_{rad}}$$

$$\frac{1}{\tau^{rad}} = A_{MD,0} \cdot n^3 \left(\frac{I_{tot}}{I_{MD}} \right) \quad (3)$$

where $A_{MD,0}$ is a constant equal to 14.65 s^{-1} and (I_{tot}/I_{MD}) the ratio of the total integrated $^5D_0 \rightarrow {}^7F_J$ emission (here taken as $J = 0$–4) to the integrated intensity of the $^5D_0 \rightarrow {}^7F_1$ transition. A threefold enhancement in Q^{Eu}_{Eu} is observed when going from H_2O (10%) to D_2O solution (33%), in line with a less-efficient nonradiative deactivation through O–D vibrations relative to O–H vibrations. The intrinsic quantum yield value for the solid-state sample (27%) is comparable to that for the D_2O solution. Replacement of D_2O by [D_6]DMSO leads to a large increase in Q^{Eu}_{Eu}, which reaches 56%. However, the overall quantum yield of the latter solution remains quite small because the energy-transfer process from the donor level of the organic chromophore to the accepting level of the Eu^{III} ion is seemingly

very inefficient. Indeed, the sensitization efficacy, calculated from [Equation (4)] is only 3–4% for the solution samples, while it increases more than 10-times for the solid-state sample to reach 43%, a reasonable value in view of the relatively large energy gap [$E_{T(0-0)}$–$E(^5D_0)$] (see above). This can be explained by the different conformations adopted by the complex in solution, relative to that in the solid state. In solution, the aromatic chromophore lies far from the Eu^{III} ion because of an "open-type" structure, while in the solid state a "closed-type" structure probably forms in which the bipyridine moieties are closer to the metal ion, henceforth facilitating energy transfer. This conformational change could be explained on the basis of the flexibility of the aliphatic ethylenediamine link between the tris-bipyridine ruthenium complex and the DOTA–Eu^{III} unit. Although detailed computational studies of the solvent and packing effects are beyond the scope of this article, it is reasonable to propose an internal hydrogen bond between the DOTA-amide carbonyl group and the NH group from the bipyridine unit; this intramolecular hydrogen bond will be favoured in the solid state, when the conformational freedom of the DOTA unit is restricted and there is no competition with intermolecular hydrogen bonds with solvent molecules. Model calculations yield $r_{Eu-L} \approx 15$ and 11 Å for the "open-" and "closed-type" structures (Scheme 4). With such distances, the main mechanism for energy transfer is likely to be of a dipole–dipole (Förster) nature. The $(1/r_{Eu-L})^{-6}$ distance dependence then predicts a 6.5-fold increase in transfer efficiency, in good qualitative agreement with the experimental values found for η_{sens}.

$$Q^{L}_{Ln} = \eta_{sens} \times Q^{Ln}_{Ln} \quad (4)$$

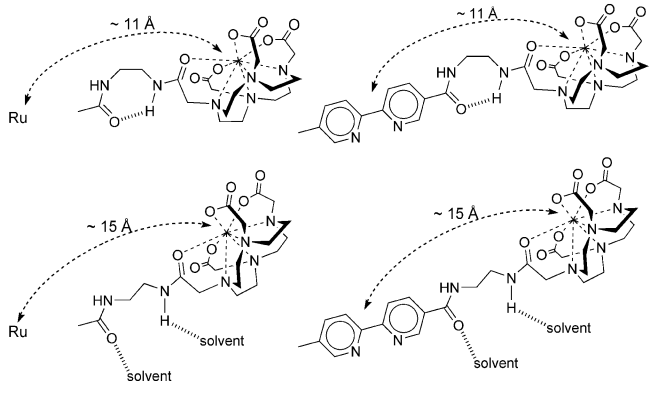

Scheme 4. Proposed conformational change for Eu_2L in the solid state through formation of an intramolecular hydrogen bond in the ethylenediamine linker, which reduces the distance between the bipyridine donor and Eu^{III} from ≈15 to ≈11 Å; the same mechanism can be invoked to explain the results with the other Ln_2L complexes and the Ln_2LRu coordination conjugates. Tentative studies were done with molecular mechanics calculations by using the SPARTAN software.

Data for Tb_2L are less informative but corroborate the interpretation made for the Eu^{III} complex. Relative intensities of the $^5D_4 \rightarrow {}^7F_J$ (J = 6–0) transitions vary little with the medium, contrary to that found for the Eu^{III} complex. Quantum yields are quite modest, in the range 1.0–2.3% (Table 2), which can probably be traced back to low sensitization efficiency of the ligands and substantial metal-to-ligand back energy transfer. Indeed, lifetimes are heavily temperature-dependent, and when the hydration number is calculated with Beeby's equation [Equation (5)],[16] a value of 1.43 is found.

$$q(\mathrm{Tb}) = 5.0\ (\Delta k_{obs} - 0.06) \quad (5)$$

A larger than expected value is typical when the quenching by O–H vibrations is not the main deactivation path in the system,[4d] in line with the expected back transfer. It is noteworthy that as for the Eu^{III} complex, single exponential decays are found for the solution samples and biexponential decays for the solid-state sample at both 295 and 77 K. In this case, however, the lifetimes are much shorter than in water probably because, similarly to the Eu^{III} complex, the solid-state conformation brings the donor "centre" closer to the metal ion, which facilitates back transfer. The calculated populations for the two coordination sites deviate somewhat from the expected 1:1 ratio (7:3), but one has to consider uncertainties both in the B_i parameters and elemental analysis.

NIR-Emitting Ln_2L Complexes

Excitation spectra of Ln_2L complexes (Ln = Nd, Yb) in solution and in the solid state present broad bands in the range 250–370 nm, which correspond to the ligand electronic transitions (Figure 4, Figures S7 and S8 in the Supporting Information). For the solid-state sample of Nd_2L, additional bands are seen which can be assigned to intraconfigurational transitions from the $Nd(^4I_{9/2})$ level to $^4F_{9/2}$ (677 nm), $^2H_{11/2}$ (622 nm), $^4G_{5/2}$, $^2G_{7/2}$ (576 nm), $^4G_{7/2}$ (523 nm), $^4G_{9/2}$ (509 nm), $^2K_{15/2}$, $^2G_{9/2}$, (^2D, $^2P)_{3/2}$, $^4G_{11/2}$, $^2P_{1/2}$ and $^2D_{5/2}$ (400–490 nm). When excited with UV light (300–330 nm), the Nd_2L and Yb_2L complexes in all media exhibit characteristic f–f emissions, $Nd(^4F_{3/2} \rightarrow {}^4I_J$, J = 9/2, 11/2, 13/2) and $Yb(^2F_{5/2} \rightarrow {}^2F_{7/2})$. Variations in the emission probabilities from different sublevels are observed in the luminescence spectra of Nd_2L when going from H_2O to DMSO solutions and to the solid state. Thus, in aqueous solution, the $^4F_{3/2} \rightarrow {}^4I_{9/2}$ and $^4F_{3/2} \rightarrow {}^4I_{11/2}$ transitions have almost equal intensities, while in DMSO and in the solid state, the last transition becomes dominant, which reflects variations in the coordination environment around Nd^{III}. The luminescence spectra of Yb_2L at room temperature are almost the same in all media, but at 77 K, variations in the ligand-field splitting of the $^2F_{7/2}$ level, as well as in the vibronic satellites accompanying this transition, are observed. For instance, the emission band for the solid-state sample is broadened in comparison with those in the solution samples, and at least 8 Stark components can be distinguished, which points to the presence of two different coordination environments. This observation is in line with that for the visible-emitting compounds. This is further confirmed by

Table 3. Lifetimes (λ_{ex} = 355 nm) and quantum yields (λ_{ex} = 330 nm) of Ln_2L (Ln = Nd, Yb) at 295 K (2σ between parentheses).

	Nd_2L		Yb_2L	
Solvent	$Q^L_{Ln} \times 10^5$	τ_{obs} [μs]	$Q^L_{Ln} \times 10^5$	τ_{obs} [μs][b]
H_2O	4.4(5)	_[a]	3.5(1)	_[a]
D_2O	19(3)	0.41(1)	17.3(1)	6.97(1)
[D_6]DMSO	24(1)	0.50(1)	68(4)	5.67(1)
Solid	23(1)	0.33(1)	27(2)	100(2), 63(4)[c] 24(1), 37(4)

[a] Not measurable. [b] Biexponential decays: population B_i given in %, see Experimental Section for discussion. [c] Biexponential decay, population B_i given in %.

the lifetime measurements. Solid-state Yb_2L exhibits biexponential decay with a quite large, longer lifetime of 100 μs (Table 3), and the population ratio 60:40 is close to 1:1. In view of the small energy gap between the emitting and ground levels, both the Nd_2L and Yb_2L lifetimes significantly increase in deuterated solvents. For Nd_2L, all of the luminescence decays were found to be monoexponential; however, the short lifetimes calculated from these decays (0.3–0.5 μs) render detection of biexponential decays difficult with our instrumentation.

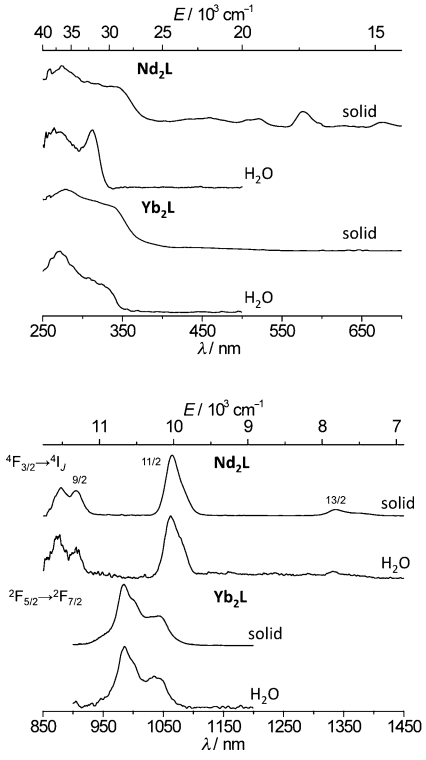

Figure 4. Corrected excitation (top, monitoring metal-centred emission) and emission (bottom) spectra of Ln_2L (Ln = Nd, Yb) at 295 K; λ_{ex} = 300–330 nm.

Quantum yields and lifetimes for Nd_2L are in the range of those usually found for complexes with organic ligands,[17] with a few exceptions.[1g] They are small owing to efficient nonradiative deactivation processes. On the other hand, quantum yields for Yb_2L are on the lower end of those reported with other organic ligands, the largest yield being recorded in [D_6]DMSO (≈0.07%), a fact we can trace back to both poor energy transfer and efficient deactivation.

Ru^{II}-Centred Absorption and Luminescence

The shape and position of the bands in the absorption spectra of H_6LRu and Ln_2LRu complexes are similar and independent of the nature of the lanthanide ion; therefore, only those for Gd^{III} will be discussed here. Absorption spectra of Gd_2LRu solutions display intense ligand-centred (LC) π→π* transitions below 220 nm and in the range 280–340 nm, as well as less intense metal-to-ligand charge transfer (^{1}MLCT) d→π* transitions at 240–270 and 390–550 nm (Figure 5). The absorption maxima of the complex in DMSO solution are redshifted by 6–10 nm. In addition, a weak band at 362 nm can be assigned to the metal-centred (MC) d→d transition of Ru^{II}. Excitation spectra of Gd_2LRu present broad bands in the range 250–600 nm with maxima at ≈270, 360, ≈450 and ≈570 nm.

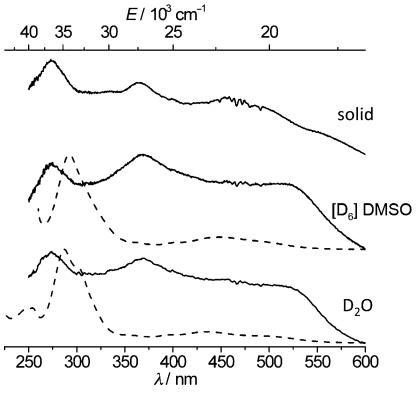

Figure 5. Corrected and normalized excitation spectra (solid lines) of Gd_2LRu in different media, with superimposed absorption spectra (dashed lines) for corresponding solutions.

Upon excitation into the ^{1}MLCT band (430–450 nm), H_6LRu and Gd_2LRu exhibit broad-band luminescence in the visible range (575–850 nm, see Figure S9, Supporting Information) further extending into the near-infrared range up to 1200 nm. At low temperature, emission spectra of

D_2O and [D_6]DMSO solutions are shifted to shorter wavelengths by ca. 100 nm; for solid-state samples, the shift is less pronounced, 20–30 nm. Decomposition of the luminescence spectra of Gd_2LRu at 77 K with Gaussian functions allows one to determine the energies of the ^{3}MLCT states (Table 4) and to deduce a general energy scheme for ligand- and Ru^{II}-centred levels (Figure 6). According to this scheme the highest-energy ^{3}MLCT level appears to be suitable for the sensitization of Nd^{III} and Yb^{III} luminescence, but lies at too low an energy for transferring its energy onto the Eu^{III} or Tb^{III} 4f excited states. The energy levels of the visible-emitting ions can therefore only be populated through ^{1}MLCT or LC $^3\pi\pi^*$ states.

Table 4. Transition energies (wavelengths) determined from absorption, emission and excitation spectra of Gd_2LRu at 77 K in different media.

H_2O/D_2O	E [cm^{-1}] (λ [nm]) [D_6]DMSO	Solid state	Assignment
>45450 (<220)	>45450 (<220)	>45450 (<220)	LC $\pi\rightarrow\pi^*$
40650 (246)	36765 (272)	36900 (271)	^{1}MLCT d$\rightarrow\pi^*$
39370 (254)			^{1}MLCT d$\rightarrow\pi^*$
35088 (285)	34364 (291)	30581 (327)	LC $\pi\rightarrow\pi^*$
32895 (304)	32258 (310)		LC $\pi\rightarrow\pi^*$
27624 (362)	27624 (362)	27624 (362)	Ru^{2+} MC d$\rightarrow$d
25316 (395)	24691 (405)	21882 (457)	^{1}MLCT d$\rightarrow\pi^*$
22883 (437)	22371 (447)	19841 (504)	^{1}MLCT d$\rightarrow\pi^*$
20040 (499)	19802 (505)	18182 (550)	^{1}MLCT d$\rightarrow\pi^*$
15688 (637)	15960 (627)	15224 (657)	^{3}MLCT
15090 (663)	15397 (649)	14716 (680)	^{3}MLCT
14164 (706)	14489 (690)	13811 (724)	^{3}MLCT
13060 (765)	13514 (740)	12912 (774)	^{3}MLCT

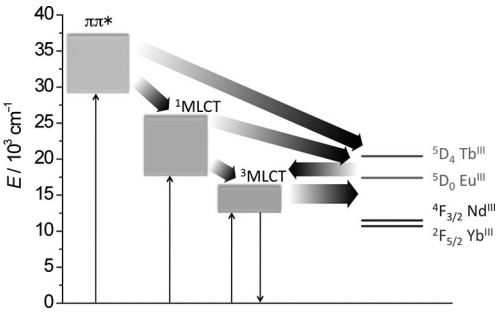

Figure 6. Energy diagram indicating the main levels and energy migration paths in Ln_2LRu.

The partial quantum yields of the Ru^{II}-centred luminescence emitted between 550 and 850 nm were determined by excitation into the ^{1}MLCT state (Table 5). Q_{Ru} is largest for the solid-state samples because of the absence of collisional deactivation; it decreases by about 30 (D_2O), 11 ([D_6]-DMSO), and 20% (solid state) in going from H_6LRu to Gd_2LRu. A more detailed analysis for the Ln_2LRu complexes will be given in the following sections.

Table 5. Quantum yields of the Ru^{II}-centred emission in H_6LRu and Ln_2LRu complexes under excitation at 437 nm and lifetimes of the Ru^{II} and Ln^{III} excited states; all data at 295 K (2σ in parentheses).

Complex	Solvent	Q_{Ru} [%][a]	τ_{Ru} [ns][b,c]	τ_{Ln} [μs][d]
H_6LRu	D_2O	0.15(1)		
Gd_2LRu		0.10(1)	16(2)	
Eu_2LRu		0.11(1)		<10 ns
Tb_2LRu		0.11(1)		[e]
Nd_2LRu		0.11(1)	17(2)	0.35(1)
Yb_2LRu		0.12(1)	18(2)	6.83(1)[f]
H_6LRu	[D_6]DMSO	0.62(2)		
Gd_2LRu		0.55(3)	727(8), 30(7) 63(4), 70(7)	
Eu_2LRu		0.54(2)		<10 ns
Tb_2LRu		0.46(3)		[e]
Nd_2LRu		0.47(2)	363(8), 6(1) 57(4), 94(1)	0.49(1)
Yb_2LRu		0.55(2)	944(9), 30(5) 81(4), 70(5)	5.13(1)
H_6LRu	solid	1.50(4)		
Gd_2LRu		1.19(1)	116(2)	
Eu_2LRu		1.13(8)		[e]
Tb_2LRu		1.07(1)		[e]
Nd_2LRu		0.29(2)	72(2)	0.21(1)
Yb_2LRu		1.29(3)	102(2)	1.85(1)

[a] Only emission in the visible range from 550 to 850 nm was considered. [b] Biexponential decays: population B_i given in %, see Experimental Section for discussion. [c] λ_{ex} = 437 nm. [d] λ_{ex} = 355 nm. [e] No Ln luminescence. [f] 1.16(3) μs in H_2O.

Ln_2LRu Complexes with Visible-Emitting Ln^{III} (Eu, Tb)

No Eu^{III}-centred luminescence is seen for the solid-state sample, regardless of the excitation wavelength. On the other hand, a characteristic f–f emission is seen in D_2O (Figure 7), which greatly depends on the excitation wavelength: the $^5D_0$ emission intensity increases when this wavelength is increased from 300 to 340 nm and then decreases upon further increase in λ_{ex} to become un-noticeable above 400 nm (Figure S10, Supporting Information). This confirms that sensitization of the Eu^{III} luminescence is possible only through the organic ligand and not by the ^{3}MLCT state. Excitation spectra, in turn, reflect this situation (Figure S11, Supporting Information): an excitation spectrum similar to that of Eu_2L is obtained upon monitoring the $^5D_0\rightarrow{}^7F_2$ hypersensitive transition (Figure 7), while monitoring of the Ru^{II} luminescence results in an excitation spectrum similar to the absorption spectrum of Ln_2LRu. The quantum yield of the Eu^{III} emission under excitation at 340 nm is 0.006(5)% only, that is ≈180 times smaller than that of Eu_2L (Table 1). The $^5D_0$ lifetime is concomitantly very short at 295 K (<10 ns); however, it increases up to 2.70(5) ms at 77 K, which indicates that the Eu^{III} luminescence is quenched at room temperature by a very efficient temperature-dependent mechanism. At 77 K (Figure 7, S12 Supporting Information), the Ru^{II}-centred emission sustains a large blueshift and almost completely overlaps with the $^5D_0\rightarrow{}^7F_J$ transitions; as a consequence, excitation spectra recorded at either 590 or 615 nm (Eu^{III}), or 640 nm

(Ru^{II}) are now superimposable. The Ru^{II} luminescence disappears under time-resolved detection with a 50-μs delay (Figure S12, Supporting Information).

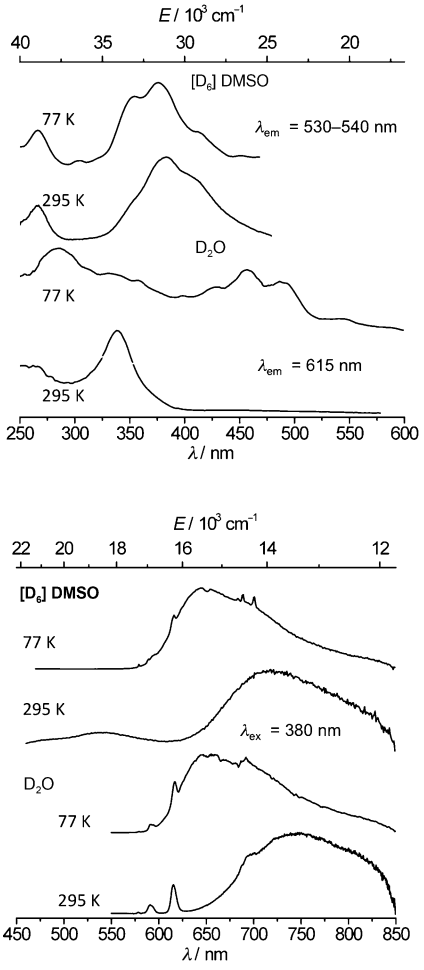

Figure 7. Upper panel: corrected excitation spectra of Eu_2LRu with the analyzing wavelength set at 615 ($^5D_0 \rightarrow {}^7F_2$ transition) or 530–540 nm. Lower panel: corresponding emission spectra (λ_{ex} = 330 nm, except otherwise stated).

In [D_6]DMSO, an unusual phenomenon occurs: no Eu^{III} emission is detectable at room temperature regardless of the excitation wavelength, but instead, a weak and broad feature appears between 480 and 600 nm, the intensity of which is dependent on λ_{ex}. The intensity of this band increases between 350 and 390 nm and then decreases and disappears for $\lambda_{ex} > 450$ nm (Figure S13, Supporting Information). The corresponding excitation spectra are shown in Figure 7 and in Figure S14, Supporting Information. When the solution is degassed with nitrogen, there is not much change in the emission intensity. On the other hand, the broad feature is no longer seen at 77 K, which is advantageous to the faint Eu^{III} emission bands superimposed on the Ru^{II} luminescence. However, the $^5D_0$ lifetime remains apparently short since no emission at all is seen after enforcing 10–50-μs time delays. A possible explanation would be the photoreduction of Eu^{III} to Eu^{II}, since such an emission band is not seen for the other Ln_2LRu complexes. The difference in behaviour as a function of temperature could be due to the blueshift of the ligand levels when the temperature is decreased. This aspect was, however, not investigated further.

As in the case of the Eu^{III} complex, the solid-state sample of Tb_2LRu does not display any f–f transitions upon excitation into the ligand or ^{3}MLCT bands, either at 295 or 77 K. This is also true for the solutions in D_2O and [D_6]-DMSO at room temperature. At 77 K, however, the $^5D_4$ emission is detected in a time-resolved mode (50-μs delay, see Figure 8), but only upon excitation into the ligand states (Figure S15, Supporting Information). Lifetimes of the $^5D_4$ level at 77 K are long, 1.61(5) and 1.66(5) ms in D_2O and [D_6]DMSO, respectively, although they are shorter than those of the Tb_2L complex (Table 2).

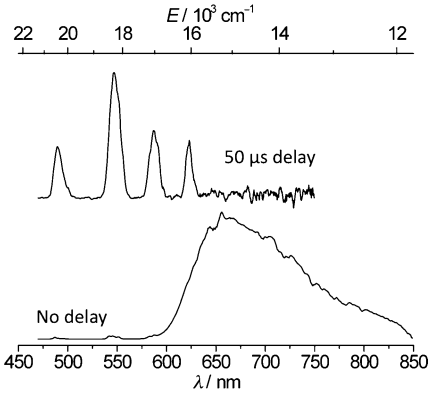

Figure 8. Emission spectra of Tb_2LRu in D_2O at 77 K without and with enforcing a 50-μs time delay; λ_{ex} = 330 nm.

The quantum yields of the Ru^{II}-centred luminescence in the Ln_2LRu solid-state samples and in [D_6]DMSO solutions (Table 5) are the same for Ln = Eu and Gd and slightly smaller for Ln = Tb. This confirms the absence of, or at most the presence of a very little, energy migration between the Ru^{II} chromophore and the Ln^{III} moieties in these heterometallic structures.

Energy Transfer in Ln_2LRu Complexes with NIR-Emitting Ln^{III} Ions (Ln = Nd, Yb)

Photophysical data for these compounds present several features. Firstly, Ru^{II} emission in the visible region is essentially the same as the emission observed for Gd_2LRu (compare Figures S9 and S16 in the Supporting Information), the only exception being the Nd_2LRu solid-state sample, for which dips in the Ru^{II} luminescence bands correspond to absorption bands of Nd^{III}, which therefore points to an energy transfer between these two moieties. Secondly, typical f–f transitions of Nd^{III} and Yb^{III} are seen in the NIR luminescence spectra for all media: $^4F_{3/2} \rightarrow {}^4I_J$ with J = 11/2 and 13/2 at 1060 and 1340 nm (the transition to J = 9/2 is obscured by Ru^{II} emission) and $^2F_{5/2} \rightarrow {}^2F_{7/2}$ at 980–1030 nm, see Figures S17 and S18 (Supporting Information). The quantitative data reported in Table 5 help to decipher the origin of the sensitization of the Ln^{III} luminescence, energy transfer from the ligand or from the Ru^{II} chromophore (^{3}MLCT).

By referring to the data for the Gd^{III} heterotrimetallic complex, it can be seen that both the quantum yield and the lifetime of the Ru^{II} emission do not vary in D_2O when going from Gd^{III} to Nd^{III} and Yb^{III}. This is also true for Yb_2LRu in [D_6]DMSO; however, here the situation is somewhat more complicated in that two lifetimes are observed for Ru^{II}, which probably arise from two differently solvated species, as postulated for the homometallic complexes (vide supra). The population ratio of the long-to-short lifetimes (70:30) is maintained between the Gd^{III} and Yb^{III} complexes, but we note an increase of 30% in both Ru^{II} lifetimes of the Yb^{III} complex relative to those of the Gd^{III} complex. We have no explanation for this; on the other hand, the quantum yield of the ruthenium luminescence remains exactly the same. For the solid-state sample, a slight increase (8%) in Q_{Ru} occurs in going from Gd^{III} to Yb^{III}, but in parallel, τ_{Ru} decreases by 12%. These fluctuations are close to experimental errors so that we can safely conclude from the set of recorded data for the Yb^{III} complex that no (or at the most, very little) energy transfer occurs from the Ru^{II} chromophore to the Yb^{III} ion. This ion is therefore excited by a mechanism similar to that in force in the homometallic Yb_2L complex. Lifetimes of the $^2F_{5/2}$ level in the two kinds of complexes are quite comparable, which points to similar coordination environments.

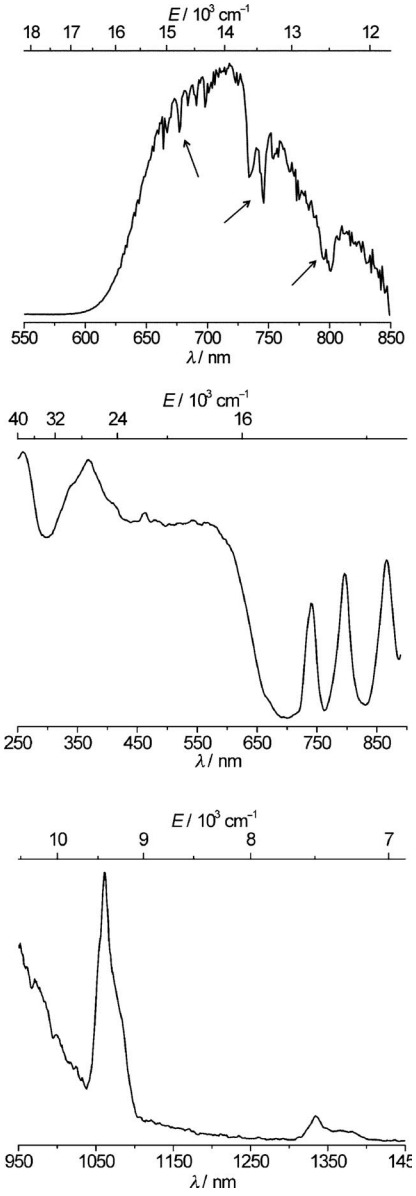

Figure 9. Solid-state sample of Nd_2LRu at 77 K: (top) Ru^{II} emission spectrum (λ_{ex} = 437 nm); middle: excitation spectrum obtained by monitoring the Nd($^4I_{15/2}\rightarrow{}^4I_{11/2}$) transition; (bottom) NIR emission spectrum under 437 nm (^{3}MLCT) excitation.

Typical spectroscopic data of a solid-state sample of Nd_2LRu are shown on Figure 9. It is noteworthy that the excitation spectrum for the Nd^{III} luminescence spans the entire visible range and the beginning of the NIR range, since the $^4F_J\leftarrow{}^4I_{9/2}$ bands are clearly seen in the range 700–850 nm. The quantum yield Q_{Ru} sustains a large decrease, from 1.19% for the Gd^{III} reference complex to 0.29%; in parallel, the τ_{Ru} lifetime also decreases, although to a lesser extent, from 116 to 102 μs. These data, together with the emission spectrum of the Ru^{II} chromophore (Figure 9, top) and the excitation spectrum (Figure 9, middle), firmly confirm energy transfer between these two moieties. The yield of the transfer can be estimated from the lifetime and quantum yield data Equation (6).

$$\eta_{et} = 1 - \frac{\tau_{obs}}{\tau_0} = 1 - \frac{Q_{obs}}{Q_0} \quad (6)$$

A yield of about 40% is calculated from the lifetime data, while the quantum yield values give a larger transfer efficiency, ≈65%. Lifetime data tend to be measured with better accuracy (a few percent) than the quantum yields (±10–20%), so that by taking the first yield into consideration, the rate of the energy transfer can be estimated by Equation (7).

$$k_{et} = 1/\tau_{RuLNd} - 1/\tau_{RuLGd} = 5.3 \times 10^6\ s^{-1} \quad (7)$$

This is relatively slow in view of the good overlap between the emission spectrum of the chromophore and the Nd^{III} absorption spectrum. However, this value is comparable to the rate reported for Ru-CH_2CH_2-Nd dyads ($2.2 \times 10^6\ s^{-1}$) in which the two bipyridyl coordinating units are separated by an ethylene bridge; when the linking unit between the two metallochromophores is conjugated, an increase in the transfer rate of up to 100-fold can be obtained.[10d]

In [D_6]DMSO, Nd_2LRu lifetimes are difficult to interpret in view of the biexponential behaviour of the luminescence decay. From the quantum yield data, a transfer efficiency of η_{et} = 15% is obtained. Again differences in the conformation of the heterometallic complex between solution and solid state can easily explain this decrease with respect to the solid-state sample.

Conclusions

Here we report a systematic and comparative photophysical study of Ln^{III} complexes and Ru^{II}–Ln^{III} coordina-

tion conjugates containing visible (Tb, Eu) or NIR-emitting (Nd, Yb) rare-earth ions. The lanthanide complexes and the heteropolymetallic conjugates derive from a ligand composed of a central bipyridine binding unit functionalized at each 5′-position with a DOTA macrocycle. The detailed luminescence studies, including quantum yield and lifetime determination, were performed in solution (water, D_2O and [D_6]DMSO) and in the solid-state and at different temperatures (295 and 77 K). All the data point to the existence of a single coordination environment for the Ln^{III} ions in solution and to two in the solid state, which can be ascribed to different hydration states. Photophysical data confirm the existence of energy transfer between the aromatic chromophore and the Ln^{III} ions in the Ln_2L lanthanide complexes, and between the $Ru(bipy)_3$ antennae and the DOTA–Nd moieties in the Nd^{III}–Ru^{II} conjugate. However, no (or at most, very little) energy transfer occurs from the Ru^{II} chromophore to the lanthanide ions in the other coordination conjugates. The differences in the emission properties of all the complexes and conjugates between the solution and solid-state samples can be justified on the basis of a change in the conformation of the supporting ligand, which influences the efficiency of the energy transfer. We are currently in the process of synthesizing other supramolecular f–d conjugates using related ligands with the aim of improving the efficiency of the energy transfer.

Experimental Section

Synthesis and Characterization: Chemicals and solvents of the highest commercial grade available were used as received. 1,4,7-Tris(*tert*-butoxycarbonylmethyl)-1,4,7,10-tetraazacyclododecane-10-acetic acid[4c] and *N*-*tert*-butoxycarbonyl-1,2-ethanediamine[11] were synthesized as described in the literature.

Compounds **4** and **6** were purified on a Büchi Sepacore preparative system consisting of a pump manager C-615 with two pump modules C-605 for binary solvent gradients, a fraction collector C-660 and a UV Photometer C-635. Purification was made by using reverse phase linear gradients of MeOH/H_2O 0.1% TFA in 30 min with a flow rate of 30 mL/min; a pre-packed preparative cartridge (150 × 40 mm) with reverse phase RP18 silica gel (Büchi order # 54863) was used. High-performance liquid chromatography (HPLC) was performed by using an Agilent 1100 series LC/MSD instrument. Analytical HPLC was run by using an Eclipse XDBC18 (4.6 × 150 mm) analytical column. Purification of the metal complexes was performed on a Zorbax ODSC18 (9.4 × 250 mm) semi-preparative reverse-phase column. Standard conditions for analytical and semi-preparative RP-HPLC consisted of an isocratic regime during the first 5 min, followed by a linear gradient from 25 to 95% of solvent B for 30 min at a flow rate of 1 mL/min (analytical) or 3 mL/min (semi-preparative); A: water with 0.1% TFA, B: methanol with 0.1% TFA.

Electrospray ionization mass spectrometry (ESI-MS) was performed on an Agilent 1100 Series LC/MSD instrument in positive scan mode by using direct injection. Elemental analyses were performed on a Carlo Erba EA 1108 analyzer. NMR spectra were recorded on a Bruker AMX-500 spectrometer, by using deuterated MeOH as solvent. IR spectra were recorded in the range 4000–600 cm^{-1} by using a Perkin–Elmer Spectrum One spectrometer equipped with a universal attenuated total reflection sampler. UV/Vis spectra were performed on a JASCO V-630 spectrophotometer equipped with a Peltier thermostat.

Ligand Synthesis

1: Potassium permanganate (21.014 g, 133.0 mmol) was dissolved in water (200 mL), and 5,5′-dimethyl-2,2′-bipyridine (5.0, 26.6 mmol) was slowly added. The reaction mixture was heated at 115 °C for 2 h and filtered through Celite. The filtrate was cooled to 5 °C in an ice–water bath, and the pH was adjusted to 3 with concentrated HCl, which resulted in the formation of a white precipitate. The precipitate was isolated by filtration and washed with water (50 mL). The wet solid was frozen and freeze–dried by using a Thermo ModulyoD drier from Thermo Scientific. Yield: 6.03 g (93%). $C_{12}H_8N_2O_4$ (244.21): calcd. C 59.0, H 3.3, N 11.5; found C 59.0, H 3.2, N 11.5. Mass spectrometry (ESI): calcd. for $C_{12}H_8N_2O_4$ $[M]^+$ 245.20); found 245.00.

3: Bipyridine **1** (1.766 g, 7.23 mmol) was dissolved in DMF (20 mL), and HATU (4.341 g, 14.47 mmol) and DIEA (12.36 mL, 70.949 mmol) were added. The bright yellow mixture was stirred for 10 min at room temperature under a nitrogen atmosphere, and then a solution of *N*-*tert*-butoxycarbonyl-1,2-ethanediamine **2** (2.544 g, 15.9 mmol) in DMF (5 mL) was added. The mixture was stirred at room temperature under a nitrogen atmosphere for 4 h. A yellow precipitate was isolated by filtration and washed with saturated NaCl (4 × 15 mL). The resulting white solid was frozen with liquid nitrogen, and freeze–dried. The purity of the solid was verified by HPLC. Yield: 2.680 g (68%). Mass spectrometry (ESI): calcd. for $C_{26}H_{36}N_6O_6$ $[M]^+$ 529.27; found 329.3.

4: Bipyridine **3** (0.529 g, 1.0 mmol) was dissolved in CH_2Cl_2 (30 mL) and TFA (30 mL, 391.77 mmol) was added. The mixture was stirred at room temperature under a nitrogen atmosphere for 4 h. The solution was concentrated under reduced pressure, washed with hexane (4 × 15 mL) and dried in vacuo. The yellow oily residue was purified on a Büchi Sepacore preparative system with MeOH/H_2O 0.1% TFA as the eluent. The purity for each fraction was checked by HPLC, and their identity was confirmed by ESI^+-MS. Collected fractions were partly concentrated under reduced pressure at 30 °C to eliminate MeOH, frozen with liquid nitrogen and freeze–dried to give the desired product as a white solid. Yield: 0.328 g (99%). Mass spectrometry (ESI): calcd. for $C_{16}H_{20}N_6O_2$ $[M]^+$ 329.37; found 329.20.

6: 1,4,7-Tris(*tert*-butoxycarbonylmethyl)-1,4,7,10-tetraazacyclododecane-10-acetic acid **5** (0.226 g, 0.288 mmol) was dissolved in DMF (20 mL); HATU (0.086 g, 0.288 mmol) and DIEA (0.92 mL, 5.281 mmol) were added. The yellow mixture was stirred for 10 min at room temperature under an inert atmosphere. A solution of bipyridine **4** (0.046 g, 0.140 mmol) in DMF (5 mL) was added. After 2 h, a second portion of HATU (0.086 g, 0.288 mmol) and DIEA (0.92 mL, 5.281 mmol) were added. The reaction mixture was stirred overnight at room temperature under a nitrogen atmosphere. The resulting dark orange solution was concentrated under reduced pressure at 70 °C. The oily residue was purified by reverse-phase chromatography. The purity for each fraction was checked by HPLC, and their identity was confirmed by ESI^+-MS. Collected fractions were partly concentrated under reduced pressure at 30 °C to eliminate MeOH, frozen and freeze–dried to give the desired product as a white solid. Yield: 0.114 g (57%). $C_{72}H_{120}N_{14}O_{16}$ (1437.82): calcd. C 60.1, H 8.4, N 13.6; found C 60.3, H 8.3, N 13.7. Mass spectrometry (ESI): calcd. for $C_{72}H_{120}N_{14}O_{16}$ $[M]^+$ 1438.81, found 1438.50; found $[M]^{2+}$ 719.00.

Ligand H_6L: Protected ligand **6** (0.100 g, 0.069 mmol) was dissolved in CH_2Cl_2 (2 mL); water (1 mL), TFA (36 mL,

470.13 mmol) and TIPS (1 mL, 4.88 mmol) were slowly added. The resulting mixture was stirred at room temperature under a nitrogen atmosphere for 24 h. The solution was then concentrated under reduced pressure, washed with hexane (3 × 15 mL) and dried in vacuo to give a pale violet powdery solid. Yield: 0.075 g (100%). $C_{48}H_{72}N_{14}O_{16}$ (1101.18): calcd. C 52.3, H 6.6, N 17.8; found C 52.2, H 6.8, N 17.8. Mass spectrometry (ESI): calcd. for $C_{48}H_{72}N_{14}O_{16}$ $[M]^+$ 1102.17, found 1101.53; found $[M]^{2+}$ 551.30. ^1H NMR (500 MHz, CD_3OD, 298 K): δ = 9.09 (s, 2 H), 8.48 (d, J = 0.016 Hz, 2 H), 8.34 (d, J = 0.017, 2 H), 3.10–4.10 (m, 56 H) ppm. UV (H_2O, 293 K): λ_{max} (ε, $M^{-1}\,cm^{-1}$) = 249 (9444), 298 (17796) nm. The purity of the solid was also verified by HPLC.

General Method for the Preparation of the Ln_2L [Ln = Nd, Eu, Tb, Gd, Yb] Complexes: Ligand H_6L (0.020 g, 0.018 mmol) was dissolved in water (15 mL), and the corresponding Ln^{III} triflate (0.11 mmol) was added. The reaction mixture was stirred at 110 °C under argon for 24 h. The solution was concentrated under reduced pressure at 50 °C, and the residue was purified by HPLC with MeOH/H_2O 0.1% TFA as eluent. The purity of each fraction was checked by HPLC, and their identity was confirmed by MS (ESI+). Collected fractions were partly concentrated under reduced pressure at 30 °C to eliminate MeOH, frozen with liquid nitrogen and then freeze–dried to give the desired product as a TFA salt.

Nd_2L: Yield: 9.6 mg (36%). $C_{48}H_{66}N_{14}Nd_2O_{16}{\cdot}H_2O$: calcd. C 41.1, H 4.9, N 14.0; found C 41.1, H 4.8, N 13.9. Mass spectrometry (ESI): calcd. for $C_{48}H_{66}N_{14}Nd_2O_{16}$ $[M]^+$ 1383.65, found 1384.10; found $[M]^{2+}$ 692.30.

Eu_2L: Yield: 9.3 mg (35%). $C_{48}Eu_2H_{66}N_{14}O_{16}{\cdot}H_2O$: calcd. C 40.7, H 4.8, N 13.8; found C 40.8, H 4.8, N 11.8. Mass spectrometry (ESI): calcd. for $C_{48}Eu_2H_{66}N_{14}O_{16}$ $[M]^+$ 1400.09, found 1400.00; found $[M]^{2+}$ 700.30.

Tb_2L: Yield: 9.0 mg (34%). $C_{48}H_{66}N_{14}O_{16}Tb_2{\cdot}H_2O$: calcd. C 40.3, H 4.8, N 13.7; found C 40.2, H 4.8, N 13.8. Mass spectrometry (ESI): calcd. for $C_{48}H_{66}N_{14}O_{16}Tb_2$ $[M]^+$ 1414.02, found 1414.80; found $[M]^{2+}$ 707.30.

Gd_2L: Yield: 9.2 mg (35%). $C_{48}Gd_2H_{66}N_{14}O_{16}{\cdot}H_2O$: calcd. C 40.4, H 4.8, N 13.7; found C 40.4, H 4.8, N 13.8. Mass spectrometry (ESI): calcd. for $C_{48}Gd_2H_{66}N_{14}O_{16}$ $[M]^+$ 1409.62, found 1409.30; found $[M]^{2+}$ 705.30.

Yb_2L: Yield: 9.8 mg (37%). $C_{48}H_{66}N_{14}O_{16}Yb_2{\cdot}H_2O$: calcd. C 39.5, H 4.7, N 13.4; found C 39.6, H 4.7, N 13.3. Mass spectrometry (ESI): calcd. for $C_{48}H_{66}N_{14}O_{16}Yb_2$ $[M]^+$ 1441.25, found 1441.40; found $[M]^{2+}$ 721.40.

General Method for the Preparation of the Ln_2LRu [Ln = Nd, Eu, Tb, Gd, Yb] Complexes: Ligand H_6L (0.020 g, 0.018 mmol) was dissolved in water (15 mL), and the corresponding Ln^{III} triflate (0.11 mmol) was added. The reaction mixture was heated at 110 °C under argon for 24 h. *cis*-Bis(2,2′-bipyridine)dichlororuthenium(II) dihydrate (0.011 g, 0.021 mmol) was added, and the resulting mixture was heated at 110 °C for 24 h under argon. The solution was concentrated under reduced pressure at 50 °C. The resulting dark violet oil was purified by HPLC. The purity of each fraction was checked by HPLC, and their identity was confirmed by MS (ESI+). Collected fractions were partly concentrated under reduced pressure at 30 °C to eliminate MeOH, frozen with liquid nitrogen and then freeze–dried. The Ru^{II} complexes were isolated as TFA salts. Orange solid. UV (H_2O, 293 K): λ_{max} (ε, $M^{-1}\,cm^{-1}$) = 286 (49653), 300 (40749), 400 (4807), 435 (6491), 500 (4096) nm.

Eu_2LRu [*cis*-Bis(2,2′-bipyridine)Ru(Eu_2L)]$^{2+}$: Yield: 11.1 mg (30%). $C_{68}Eu_2H_{82}N_{18}O_{16}Ru{\cdot}H_2O{\cdot}(CF_3COO)_2$: calcd. C 42.0, H 4.1, N 12.2; found C 42.1, H 4.2, N 12.1. Mass spectrometry (ESI): calcd. for $C_{68}Eu_2H_{82}N_{18}O_{16}Ru$ $[M]^{2+}$ 906.24; found 906.70.

Tb_2LRu [*cis*-Bis(2,2′-bipyridine)Ru(Tb_2L)]$^{2+}$: Yield: 10.5 mg (29%). $C_{68}H_{82}N_{18}O_{16}RuTb_2{\cdot}H_2O{\cdot}(CF_3COO)_2$; calcd. C 41.8, H 4.1, N 12.2; found C 41.8, H 4.0, N 12.1 Mass spectrometry (ESI): calcd. for $C_{68}H_{82}N_{18}O_{16}RuTb_2$ $[M]^{2+}$ 913.20; found 913.00.

Yb_2LRu [*cis*-Bis(2,2′-bipyridine)Ru(Yb_2L)]$^{2+}$: Yield: 9.8 mg (26%). $C_{68}H_{82}N_{18}O_{16}RuYb_2{\cdot}H_2O{\cdot}(CF_3COO)_2$: calcd. C 41.2, H 4.0, N 12.0; found C 41.3, H 4.1, N 11.9. Mass spectrometry (ESI): calcd. for $C_{68}H_{82}N_{18}O_{16}RuYb_2$ $[M]^{2+}$ 927.32; found 927.40.

Nd_2LRu [*cis*-Bis(2,2′-bipyridine)Ru(Nd_2L)]$^{2+}$: Yield: 11.3 mg (31%). $C_{68}H_{82}N_{18}Nd_2O_{16}Ru{\cdot}(H_2O)_2{\cdot}(CF_3COO)_2$: calcd. C 42.0, H 4.2, N 12.2; found C 42.1, H 4.2, N 12.1. Mass spectrometry (ESI): calcd. for $C_{68}H_{82}N_{18}Nd_2O_{16}Ru$ $[M]^{2+}$ 898.50; found 898.40.

Gd_2LRu [*cis*-Bis(2,2′-bipyridine)Ru(Gd_2L)]$^{2+}$: Yield: 10.9 mg (30%). $C_{68}Gd_2H_{82}N_{18}O_{16}Ru{\cdot}H_2O{\cdot}(CF_3COO)_2$: calcd. For C 41.8, H 4.1, N 12.2; found C 41.8, H 4.1, N 12.3. Mass spectrometry (ESI): calcd. for $C_{68}Gd_2H_{82}N_{18}O_{16}Ru$ $[M]^{2+}$ 911.53; found 911.80.

H_6LRu [*cis*-Bis(2,2′-bipyridine)Ru(H_6L)]$^{2+}$: Ligand H_6L (0.040 g, 0.036 mmol) was dissolved in EtOH (15 mL), and $Ru(Bipy)_2Cl_2$ (0.022 g, 0.043 mmol) was added. The reaction mixture was heated at 90 °C for 12 h under argon. The solution was concentrated under reduced pressure at 50 °C. The resulting dark violet oil was purified by HPLC with MeOH/H_2O 0.1% TFA. The purity of each fraction was checked by analytical HPLC, and their identity was confirmed by MS (ESI+). Collected fractions were partly concentrated under reduced pressure at 30 °C to eliminate the MeOH, frozen with liquid nitrogen, and then freeze–dried. The Ru^{II} complex was isolated as a TFA salt. Orange solid. Yield: 10.3 mg (33%). $C_{68}H_{88}N_{18}O_{16}Ru{\cdot}(CF_3COO)_2$: calcd. C 49.7, H 5.1, N 14.5; found C 49.8, H 5.1, N 14.6. Mass spectrometry (ESI): [calcd. for $C_{68}H_{88}N_{18}O_{16}Ru$ $[M]^{2+}$ 757.30; found 757.40. ^1H NMR (500 MHz, CD_3OD, 298 K): δ = 8.91 (s, 2 H), 8.69 (m, 4 H), 8.51 (s, 2 H), 8.10 (m, 6 H), 7.82 (m, 4 H), 7.48 (m, 4 H), 2.90–4.00 (m, 56 H) ppm.

Photophysical Measurements: Low-resolution luminescence data (spectra and lifetimes in the visible range) were obtained by using a Fluorolog FL3–22 spectrofluorimeter from Horiba-Jobin–Yvon Ltd. For emission in the near-infrared spectral range the spectrometer was fitted with a second measuring channel equipped with a FL-1004 single-grating monochromator, and the light intensity was measured by (i) a DSS-IGA020L Jobin–Yvon solid-state InGaAs detector cooled to 77 K (range 800–1600 nm) or (ii) a NIR photomultiplier Hamamatsu H9170–75 cooled by the Peltier effect at –60 °C (range 930–1700 nm). All emission and excitation spectra were corrected for the instrumental functions. Lifetimes are averages of at least three independent measurements. Samples were placed into special 2.4-mm i.d. quartz capillaries; measurements at 77 K were performed on frozen solutions to which 10% of glycerol was added. Lifetimes in the NIR spectral range and for the solid-state samples of Ln_2L (Ln = Eu, Tb) were measured upon excitation at 355 nm provided by a Quantel Brillant Nd:YAG laser equipped with a frequency tripler. The output signal of the NIR or visible photomultiplier was fed into a Stanford Research SR-430 multichannel scaler and transferred to a PC. Lifetimes of the Ru^{II} emission were measured under excitation at 437 nm from an Ekspla NT 342/3/UV setup and analyzed with a Hamamatsu C8808 photonic multichannel analyzer. Quantum yields were determined with a Fluorolog FL3–22 spectrofluorimeter at room temperature, under excitation into ligand (300–330 nm) or Ru^{II}-based (437 nm) states, according to an absolute method[18] by using a home-modified inte-

gration sphere.[19] Each sample was measured several times under slightly different experimental conditions. The estimated accuracy for quantum yields is ±10–20%. High-resolution excitation spectra for Eu^{III} complexes in the range of the $^5D_0 \leftarrow {}^7F_0$ transition were measured by using a tuneable Coherent CR-599 dye laser (band path 0.03 nm, 50–300 mW) pumped by a continuous Coherent Innova-90 argon laser (8 W) as an excitation source equipped with a specially designed stepper motor; the emitted light was analyzed in the range 610–620 nm with a wide-band gap monochromator from ORIEL (model 77250). A more detailed description of the experimental procedure can be found in ref.[20] Concentrations of the solutions in the various solvents were between 1.6 and 3.0 mM.

Note on Lifetime Determinations: Some decays could not be fitted with single exponential functions. For Eu_2L, differences between mono- and biexponential fits were rather small, but the recalculated decays with two lifetimes definitively matched the experimental data better, as indicated by the statistical tests (Figure 10). For biexponential decays, the following equations were used, where B_i is the population of sites with lifetime τ_i, and $<\tau>$ is the mean lifetime.

$$I = I_0 + A_1 \cdot e^{-t/\tau_1} + A_2 \cdot e^{-t/\tau_2}$$

$$B_i = \tau_i A_i / \sum_i \tau_i A_i$$

$$<\tau> = \sum B_i \tau_i^2 / \sum B_i \tau_i$$

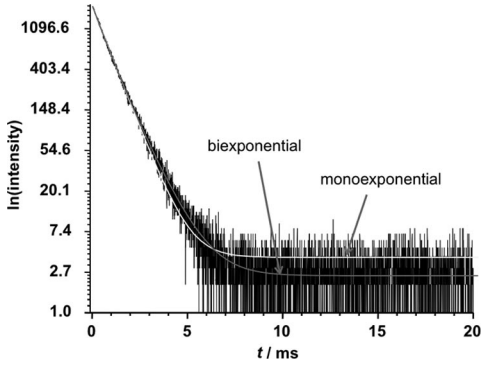

Figure 10. Typical analysis of the luminescence decay of a solid-state sample of Eu_2L. χ^2 = 418.9 and 303.6, R^2 = 0.9986 and 0.9990 for mono and biexponential fits.

Supporting Information (see footnote on the first page of this article): Energies of phonon transitions in the phosphorescence spectra of Gd_2L complexes (Table S1), relative integral intensities of f–f transitions of Eu_2L (Table S2) and Tb_2L (Table S3), energies of 0–0 transitions of Eu_2L (Table S4), and IR spectra of the organic ligand and all the complexes (Figures S1, S2), emission spectra demonstrating the effect of UV irradiation (Figures S3, S4), excitation and/or emission spectra of the Ln_2L (Ln = Nd, Eu, Tb, Yb), H_6LRu and Ln_2LRu (Ln = Nd, Gd, Yb) complexes at 77 and 295 K in different media (Figures S5–S9, S16–S18), emission (with and without enforcing a 50-μs delay) and excitation spectra of Ln_2LRu (Ln = Eu, Tb) in D_2O and [D_6]DMSO depending on the excitation or emission wavelengths (Figures S10–S15).

Acknowledgments

The Directorate-General for Research and Development of the Xunta of Galicia (PGIDIT06PXIB209055PR and INCITE09 209 084 PR) and the Ministry for Science and Innovation of Spain (CTQ2009-14431/BQU and Consolider Ingenio 2010 CSD2007-00006) funded this work. M. V. L. and M. E. V. thank the Ministry for Science and Innovation of Spain for their "Ramón y Cajal" contracts. M. V. L. also thanks the Directorate-General for Research and Development of the Xunta of Galicia for a short research stay grant at the Ecole Polytechnique Fédérale de Lausanne. G. R. thanks the International Iberian Nanotechnology Laboratory for a PhD grant. S. E. thanks the Swiss National Science Foundation for a grant (200020_119866/1). J. C. B. thanks the World Class University program from the Ministry of Education, Science, and Technology of South Korea for a grant (R31-10035). We also thank Frédéric Gumy and Julien Andrès for their help in recording some luminescence data.

[1] a) D. Parker, R. S. Dickins, H. Puschmann, C. Cossland, J. A. K. Howard, *Chem. Rev.* **2002**, *102*, 1977–2010; b) H. Tsukube, S. Shinoda, *Chem. Rev.* **2002**, *102*, 2389–2404; c) H. Tsukube, S. Shinoda, H. Tamiaki, *Coord. Chem. Rev.* **2002**, *226*, 227–234; d) J.-C. G. Bünzli, *Acc. Chem. Res.* **2006**, *39*, 53–61; e) G. Accorsi, A. Listori, K. Yoosaf, *Chem. Soc. Rev.* **2009**, *38*, 1690–1700; f) C. Andraud, O. Maury, *Eur. J. Inorg. Chem.* **2009**, 4357–4371; g) S. V. Eliseeva, J.-C. G. Bünzli, *Chem. Soc. Rev.* **2010**, *39*, 189–227.

[2] Y. Hasegawa, T. Ohkubo, K. Sogabe, Y. Kawamura, Y. Wada, H. Nakashima, S. Yanagida, *Angew. Chem. Int. Ed.* **2000**, *39*, 357–360.

[3] a) L. H. Slooff, A. Polman, M. P. Oude Wolbers, F. C. J. van Veggem, D. N. Reinhoudt, J. W. Hofstraat, *J. Appl. Phys.* **1998**, *83*, 497–503; b) L. H. Sloof, A. Polman, S. I. Klink, G. A. Hebbink, L. Grave, F. C. J. M. van Veggel, D. N. Reinhoudt, J. W. Hofstraat, *Opt. Mater.* **2000**, *14*, 101–107.

[4] a) I. Hemmilä, V. M. Mukkala, *Crit. Rev. Clin. Lab. Sci.* **2001**, *38*, 441–519; b) L. Vázquez-Ibar, A. B. Weinglass, H. R. Kaback, *Proc. Natl. Acad. Sci. USA* **2002**, *99*, 3487–3492; c) E. Pazos, D. R. Torrecilla, M. Vázquez López, L. Castedo, J. L. Mascareñas, A. Vidal, M. E. Vázquez, *J. Am. Chem. Soc.* **2008**, *130*, 9652–9653; d) E. Deiters, B. Song, A.-S. Chauvin, C. D. B. Vandevyver, F. Gumy, J.-C. G. Bünzli, *Chem. Eur. J.* **2009**, *15*, 885–900; e) V. Fernández-Moreira, B. Song, V. Sivagnanam, A.-S. Chauvin, C. D. B. Vandevyver, M. Gijs, I. Hemmilä, H.-A. Lehr, J.-C. G. Bünzli, *Analyst* **2010**, *135*, 42–52.

[5] a) S. Faulkner, J. L. Matthews in *Comprehensive Coordination Chemistry II* (Ed.: M. D. Ward), Elsevier B. V., Amsterdam, **2003**, vol. 9, ch. 9.21, pp. 913–944; b) T. Gunnlaugsson, J. P. Leonard, *Chem. Commun.* **2005**, 3114–3131; c) T. Gunnlaugsson, F. Stomeo, *Org. Biomol. Chem.* **2007**, *5*, 1999–2009.

[6] a) C. Piguet, J.-C. G. Bünzli, *Chem. Soc. Rev.* **1999**, *28*, 347–358; b) J.-C. G. Bünzli, C. Piguet, *Chem. Rev.* **2002**, *102*, 1977–2010; c) S. Faulkner, S. J. A. Pope, *J. Am. Chem. Soc.* **2003**, *125*, 10526–10527; d) D. Imbert, M. Cantuel, J.-C. Bünzli, C. Bernardinelli, C. Piguet, *J. Am. Chem. Soc.* **2003**, *125*, 15698–15699; e) J.-C. G. Bünzli, C. Piguet, *Chem. Soc. Rev.* **2005**, *34*, 1048–1077; f) S. Faulkner, B. P. Burton-Pye, *Chem. Commun.* **2005**, 259–261; g) M. D. Ward, *Coord. Chem. Rev.* **2007**, *251*, 1663–1677; h) S. Faulkner, L. S. Natrajan, W. S. Perry, D. Sykes, *Dalton Trans.* **2009**, 3890–3899; i) C. Piguet, J.-C. G. Bünzli in *Handbook on the Physics and Chemistry of Rare Earths* (Eds.: K. A. Gschneidner Jr., J.-C. G. Bünzli, V. Pecharsky), Elsevier Science B. V., Amsterdam, **2010**, vol. 40, ch. 247, pp. 351–553.

[7] a) P. B. Glover, P. R. Aston, L. J. Childs, A. Rodger, M. Kercher, R. M. Williams, L. De Cola, Z. Pikramenou, *J. Am. Chem. Soc.* **2003**, *125*, 9918–9919; b) P. A. Bassett, S. W. Magennis, P. B. Glover, D. J. Lewis, N. Spencer, S. Parson, R. M. Williams, L. De Cola, Z. Pikramenou, *J. Am. Chem. Soc.* **2004**, *126*, 9413–9424; c) G. M. Davis, S. J. A. Pope, H. Adams, S. Faulkner, M. D. Ward, *Inorg. Chem.* **2005**, *44*, 4656–4665.

[8] a) J. Van Houten, R. J. Watts, *J. Am. Chem. Soc.* **1976**, *98*, 4853–4858; b) J. Van Houten, R. J. Watts, *Inorg. Chem.* **1978**,

17, 3381–3385; c) B. Durham, J. V. Caspar, J. K. Nagle, T. J. Meyer, *J. Am. Chem. Soc.* **1982**, *104*, 4803–4810.

[9] a) S. I. Klink, H. Keizer, F. C. J. M. van Veggel, *Angew. Chem. Int. Ed.* **2000**, *39*, 4319–4321; b) C. Giansante, P. Ceroni, V. Balzani, F. Vögtle, *Angew. Chem. Int. Ed.* **2008**, *47*, 5422–5425.

[10] a) K. Senéchal-David, S. J. A. Pope, S. Quinn, S. Faulkner, T. Gunnlaugsson, *Inorg. Chem.* **2006**, *45*, 10040–10042; b) S. G. Baca, H. Adams, D. Sykes, S. Faulkner, M. D. Ward, *Dalton Trans.* **2007**, 2419–2430; c) T. Lazarides, H. Adams, D. Sykes, S. Faulkner, G. Calogero, M. D. Ward, *Dalton Trans.* **2008**, 691–698; d) T. Lazarides, D. Sykes, S. Faulkner, A. Barbieri, M. D. Ward, *Chem. Eur. J.* **2008**, *14*, 9389–9399; e) A. M. Nonat, S. J. Quinn, T. Gunnlaugsson, *Inorg. Chem.* **2009**, *48*, 4646–4648; f) T. Lazarides, N. M. Tart, D. Sykes, S. Faulkner, A. Barbieri, M. D. Ward, *Dalton Trans.* **2009**, 3971–3979; g) L. Moriggi, A. Aebischer, C. Cannizzo, A. Sour, A. Borel, J.-C. G. Bünzli, L. Helm, *Dalton Trans.* **2009**, 2088–2095.

[11] M. Vázquez López, M. E. Vázquez, C. Gómez-Reino, R. Pedrido, M. R. Bermejo, *New J. Chem.* **2008**, *32*, 1473–1477.

[12] a) S. Aime, M. Botta, M. Fasano, M. P. M. Marques, C. F. G. C. Geraldes, D. Pubanz, A. E. Merbach, *Inorg. Chem.* **1997**, *36*, 2059–2068; b) M. Meyer, V. Dahaoui-Gindrey, C. Lecomte, L. Guilard, *Coord. Chem. Rev.* **1998**, *180*, 1313–1405; c) R. Delgado, V. Félix, L. M. P. Lima, D. W. Price, *Dalton Trans.* **2007**, 2734–2745.

[13] J.-C. G. Bünzli, S. V. Eliseeva in *Springer Series on Fluorescence, Vol. 8, Lanthanide Spectroscopy, Materials, and Bio-applications*, Springer Verlag, Berlin, **2010**, published online July 15, DOI: 10.1007/4243_2010_3.

[14] S. T. Frey, W. deW. Horrocks Jr., *Inorg. Chim. Acta* **1995**, *229*, 383–390.

[15] J.-C. G. Bünzli, J.-P. Metabanzoulou, P. Froidevaux, L. Jin, *Inorg. Chem.* **1990**, *29*, 3875–3881.

[16] A. Beeby, I. M. Clarkson, R. S. Dickins, S. Faulkner, D. Parker, L. Royle, A. S. de Sousa, J. A. G. Williams, M. Woods, *J. Chem. Soc. Perkin Trans. 2* **1999**, 493–504.

[17] S. Comby, J.-C. G. Bünzli in *Handbook on the Physics and Chemistry of Rare Earth* (Eds.: K. A. Gschneidner Jr., J.-C. G. Bünzli, V. Pecharsky), Elsevier Science Publ., Amsterdam, **2007**, vol. 37, ch. 235, pp. 217–470.

[18] J. N. Demas, G. A. Crosby, *J. Phys. Chem.* **1971**, *75*, 991–1024.

[19] A. Aebischer, F. Gumy, J.-C. G. Bünzli, *Phys. Chem. Chem. Phys.* **2009**, *11*, 1346–1353.

[20] S. Comby, D. Imbert, A.-S. Chauvin, J.-C. G. Bünzli, *Inorg. Chem.* **2006**, *45*, 732–743.

Received: May 11, 2010
Published Online: August 16, 2010

